

Tough, Rapidly Swelling Thermoplastic Elastomer Hydrogels for Hemorrhage Control

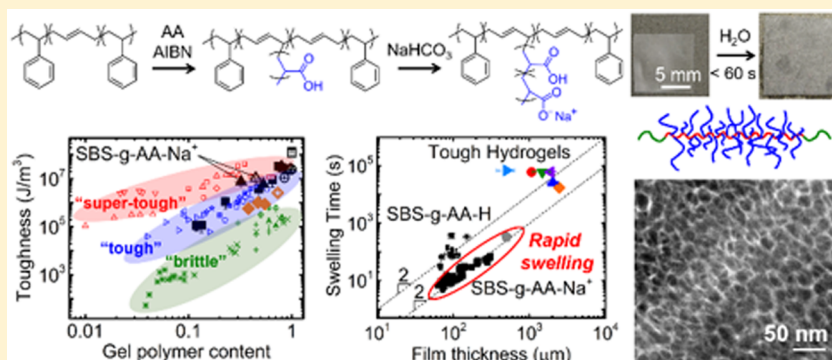
Erich D. Bain,^{†,‡} Tyler R. Long,[†] Frederick L. Beyer,^{†,§} Alice M. Savage,^{†,¶} Mark D. Dadmun,^{‡,§,¶} Halie Martin,[‡] Joseph L. Lenhart,^{*,†} and Randy A. Mrozek^{*,†}

[†]U.S. Army Research Laboratory, Aberdeen Proving Ground, Maryland 21005, United States

[‡]Department of Chemistry, University of Tennessee, Knoxville, Tennessee 37996, United States

[§]Chemical Sciences Division, Oak Ridge National Laboratory, Oak Ridge, Tennessee 37831, United States

Supporting Information



ABSTRACT: We present a novel elastomer with an amphiphilic triblock/graft architecture, allowing it to rapidly swell in water and form a tough hydrogel. The design was motivated by uncontrolled hemorrhage, responsible for 80–90% of potentially survivable deaths of US soldiers over the past 15 years. The polymer is 5.7 times as absorbent and 3 times as tough as a state of the art gauze-based hemostatic dressing. It swells to equilibrium within seconds in phosphate buffered saline due to a microphase-separated morphology featuring a continuous mobile ionic phase supported by hydrophobic glassy domains and rubbery linkages, as observed by transmission electron microscopy and small-angle neutron scattering. Thickness-dependent swelling is as much as an order of magnitude faster than many tough hydrogels in the literature, yet toughness is comparable as a function of water content. The polymer is combined with gauze to form a rapidly swelling, fiber-reinforced hydrogel composite with promising mechanical properties.

1. INTRODUCTION

Despite unprecedented improvements in battlefield injury survivability, uncontrolled hemorrhage remains the leading cause of preventable military deaths and a leading cause of preventable civilian death following trauma.^{1–4} Between 2001 and 2011, hemorrhage was responsible for 90% of prehospital battlefield deaths deemed “potentially survivable” (PS) by a review panel from the US Army Institute of Surgical Research.¹ The majority occurred due to blast or projectile penetration into trunk or junctional regions,^{1,2} which cannot be isolated by tourniquet. Many advanced hemostatic agent candidates have been developed over the past 15 years to address these issues, including HemCon and QuikClot, which were rapidly deployed by US military forces in the early 2000s despite minimal clinical testing.^{3,5} Field results were mixed, and a second generation soon followed including granular agents based on chitosan (Celox) or smectite clay (Woundstat) as well as a kaolin clay-impregnated gauze from the makers of QuikClot, dubbed Combat Gauze.

Prehospital hemostatic dressing candidates are subject to a rigorous set of criteria, including rapid stoppage of massive bleeding from severe arterial and venous injuries, simplicity of use, conformability to many wound types, safe and easy removal, light weight, durability in storage, and low cost.^{3,6,7} Many advanced candidates^{8–15} with demonstrated ability to stop bleeding in animal models have not yet been adopted by militaries, for reasons including cost, complexity of storage, need for preparatory steps, and difficulties associated with applying a liquid into a massively bleeding penetration wound.

In a lethal arterial groin puncture wound in swine, the granular agents Woundstat and Celox outperformed eight other battlefield hemostat candidates by several metrics including survival.¹⁶ These agents are able to conform to a variety of wound geometries and rapidly absorb a large amount of blood. The authors deemed both of these aspects critical to seal the

Received: February 26, 2018

Revised: May 30, 2018

Table 1. Formulation of Three Series of SBS-g-AA Graft Copolymers^a

sample (g AA-series)	SBS backbone	AA (g)	AIBN (g)	$[AA]_0$ (mol L ⁻¹)	$[AIBN]_0$ (mmol L ⁻¹)	$[AA]_0/[AIBN]_0^{0.5}$	PAA M_n^b (kDa)	PAA M_w^b (kDa)	DI water U_E (wt %)
10-1	V8508A	10	0.5059	0.53	11.9	4.9	1.5 ± 1.5	4.6 ± 3.5	25 ± 1
25-1	V8508A	25	0.3514	1.27	7.8	14.3	7.3 ± 0.1	15.4 ± 4.1	340 ± 6
35-1	V8508A	35	0.1265	1.71	2.7	32.9	10.1 ± 0.8	18.8 ± 5.2	650 ± 45
40-1	V8508A	40	0.100	1.93	2.1	41.9	9.8 ± 2.6	22 ± 9.3	742 ± 11
10-2	V8508A	10	0.5059	0.53	11.9	4.9	0.7 ± 0.7	3.4 ± 3.0	36 ± 2
15-2	V8508A	15	0.2846	0.79	6.6	9.7	1.8 ± 1.1	5.6 ± 3.0	133 ± 37
25-2	V8508A	25	0.3514	1.27	7.8	14.3	2.2 ± 1.5	6.1 ± 3.0	210 ± 7
30-2	V8508A	30	0.1821	1.49	4.0	23.7	1.6 ± 1.5	5.4 ± 3.0	161 ± 9
40-2	V8508A	40	0.100	1.93	2.1	41.9	5.6 ± 1.5	11.7 ± 3.0	492 ± 121
10-3	V6241A	10	0.5059	0.53	11.9	4.9	2.4 ± 2.4	3.9 ± 3.9	3 ± 2
40-3	V6241A	40	0.100	1.93	2.1	41.9	3.4 ± 0.9	6.1 ± 0.6	123 ± 5

^aAll formulations consisted of 6 g of SBS in 250 mL of THF along with other reactants listed, degassed, and heated to reflux for 24 h. ^bEstimated by correlating SEC-CC measurements to MD-SEC of PAA polymerized without SBS; see Supporting Information section S1 for details.

wound and stop bleeding quickly, enabling slower clot-promoting mechanisms to function effectively. However, granular agents are difficult to fully remove, and in one study Woundstat infiltrated the circulatory system of swine, causing vessel occlusion and embolism.¹⁷ Therefore, gauze-based hemostats, including Combat Gauze as well as chitosan-impregnated dressings, are currently considered state of the art due to a combination of safety and effectiveness.^{3,16,17} Gauze provides several benefits: (a) a compliant substrate for conformability to various wound geometries, (b) absorption of blood by wicking or swelling, and (c) mechanical cohesion (toughness), facilitating safe and complete removal of the hemostat following treatment. Nevertheless, an early form of Combat Gauze labeled “X-sponge” absorbed less than half as much blood as Celox and Woundstat, leading to a lower survival rate.¹⁶ Therefore, a substrate that swells to a greater extent in blood, but remains sufficiently tough to allow safe removal, is expected to improve hemostatic effectiveness, independent of the incorporated clotting mechanisms.

Given the need for high absorbency and toughness, it is natural to consider so-called “tough hydrogels”^{18–23} as a potential component in these dressings. Recent work on fiber-reinforced tough hydrogels^{23–27} suggests improved performance could be achieved by embedding a gauze-like fiber network in a flexible matrix which swells rapidly in contact with blood. Such a material in the form of a flexible dry tape may offer an improved substrate for kaolin, chitosan, or other advanced hemostatic agents currently supplied on gauze alone. However, reported swelling time scales for tough hydrogels such as “double networks”,²⁸ acrylamide-alginate,²¹ and polyampholytes²² are typically on the order of days or weeks, much too slow to stabilize an exsanguinating wound. Additionally, common tough hydrogel components such as polyacrylamide are brittle solids in the dry state, limiting their ability to conform to varying wound geometries.

Based on the above considerations, an ideal substrate for a prehospital battlefield hemostatic dressing would be one that is flexible and conformable when dry, rapidly uptakes large amounts of water in a blood-like environment, and remains tough while swollen. In this paper we present a rapidly swelling tough hydrogel platform based on simple chemical modification of the commodity thermoplastic elastomer polystyrene-polybutadiene-polystyrene (SBS) triblock copolymer. This material exceeds the performance of a state of the art gauze-based hemostatic dressing relative to these goals, as shown

using thickness-dependent absorption tests and uniaxial tensile testing. Furthermore, the material can be combined with gauze to form a fiber-reinforced hydrogel composite with promising swelling and mechanical properties. Transmission electron microscopy and small-angle neutron scattering are used to show that these properties arise from a microphase-separated morphology that facilitates both rapid swelling and mechanical cohesion.

2. EXPERIMENTAL SECTION

2.1. Materials. Vector 8508A and Vector 6241A are antioxidant-free grades of polystyrene–polybutadiene–polystyrene triblock copolymer (SBS), provided by Dexco Polymers and used as received. Azobis(isobutyronitrile) (AIBN) was recrystallized from methanol and stored at 2 °C until use. Acrylic acid was passed through a basic alumina plug to remove inhibitor prior to use. Deionized water (DIW) of 18 MΩ resistivity was produced by a Milli-Q filtration system (Millipore Corporation). QuikClot Advanced Clotting Gauze (ACG) was obtained from Adventure Medical Kits and used as received. All other chemicals were obtained from major suppliers (Sigma-Aldrich, VWR, or Fischer Scientific) and used as received unless otherwise noted.

2.2. Polymerization. 6 g of SBS was dissolved in 250 mL of tetrahydrofuran. Desired amounts of acrylic acid (AA) and azobisisobutyronitrile (AIBN) (see Table 1) were added, and the solution was degassed by three freeze–pump–thaw cycles. The solution was refluxed under a nitrogen atmosphere for 24 h, after which approximately half the solvent was removed by a rotovap. Chilled methanol was added, causing precipitation of a rubbery white solid which was immersed in refluxing methanol in a Soxhlet extractor for 24 h and then dissolved in a 95/5 THF/water (v/v) mixture via Soxhlet extraction for 8 h. Excess water was removed from the solution by three cycles of evaporation and redissolution in THF.

2.3. Size Exclusion Chromatography (SEC). PAA and SBS-g-AA samples were dried to constant mass and dissolved in HPLC-grade THF to make a 15 mg/mL solution. After passing through a 0.15 μm PTFE syringe filter, 100 μL of each solution was injected onto an Agilent 1260 Infinity HPLC system pumping THF at 1.0 mL/min through two Varian PLGel 5 μm Mixed D columns followed by a Wyatt DAWN Heleos-II multiangle light scattering detector and Wyatt Optilab rEX differential refractive index (dRI) detector. Absolute molecular weight (M) values were calculated using both detectors assuming 100% mass recovery to calculate dn/dc from the dRI traces. For relative M by conventional calibration (SEC-CC), columns were calibrated using Viscotek PolyCAL polystyrene standards with peak M of 1050, 2790, 6040, 13 400, and 19 000 Da, using a linear calibration between retention volume and log M to achieve the best fit over this molecular weight range.

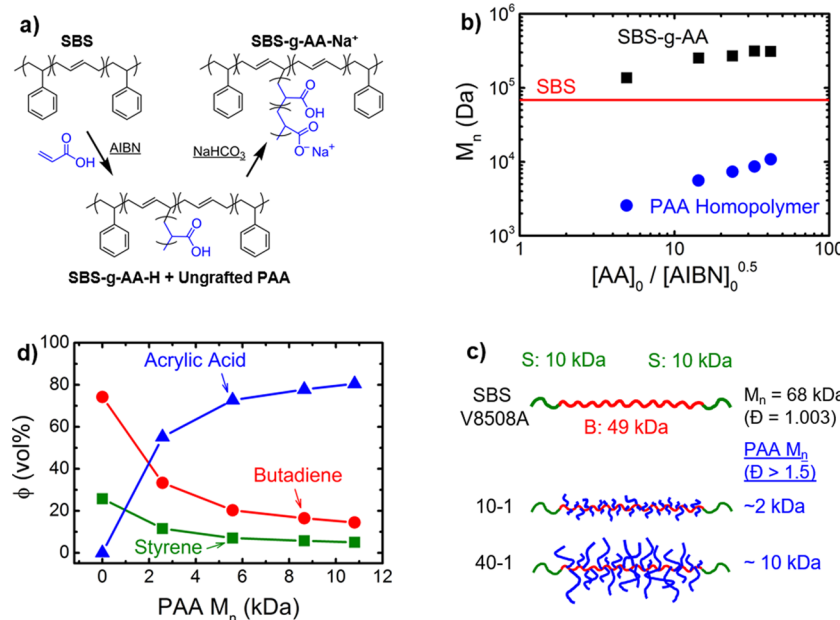


Figure 1. Preparation and molecular characterization of SBS-g-AA. (a) Synthetic scheme showing graft polymerization and sodium bicarbonate treatment. (b) Number-average molecular weights of SBS, SBS-g-AA copolymers, and ungrafted PAA measured by multidetector SEC, proportional to kinetic chain length according to free-radical polymerization kinetic theory. (c) Scheme of SBS and SBS-g-AA with low (~2 kDa) and high (~10 kDa) graft molecular weight. (d) Estimated volume fractions of styrene (S), butadiene (B), and acrylic acid, assuming constant graft density of 28 PAA chains/SBS backbone.

2.4. Film Casting and Salt Treatment. SBS-g-AA solutions in THF were diluted to 100 mg/mL and cast onto glass plates using a doctor blade set to 0.94 mm height. Films were covered with a loose-fitting lid and allowed to dry overnight, then air-dried uncovered 1–2 h, then dried under vacuum at 35 °C for 3–5 h. Films of varying thickness were formed by casting multiple layers of material on top of one another with 40–60 min air drying under a propped-up Petri dish between each casting. Films for TEM and SANS were covered by a Petri dish flush with the glass substrate, with one small reservoir each of water and THF inside the dish, and left overnight, after which the solvents were evaporated and the films were dry to the touch. They were air-dried uncovered for several hours and then vacuum-dried as above. Dried films were immersed in deionized water (DIW) to aid removal from the glass. Selected films were then immersed and shaken in saturated aqueous sodium bicarbonate, 15 mM calcium hydroxide, or 15 mM zinc acetate for 1 h to form the Na⁺, Ca²⁺, or Zn²⁺ salt of poly(acrylic acid), respectively. This was followed by three successive 1 h shakings in DI water to remove excess salt. Films were hung up to air-dry and then vacuum-dried overnight at 50 °C. Film thickness was measured using a micrometer (Mitutoyo) to $\pm 0.5\text{ }\mu\text{m}$ accuracy. Tensile test specimens were punched out using a hydraulic press and standard dies.

2.5. Advanced Clotting Gauze (ACG) Composites. ACG/SBS-g-AA composites were formed by casting THF solutions of SBS-g-AA onto as-received sheets of ACG on a glass plate and covering overnight. Composites were dried and converted to sodium salt in the same way as neat polymer films. Fiber mass fractions M_f were estimated by weighing three 1 cm squares each of ACG and the composite, using the formula $M_f = m_{\text{ACG}}/m_c$, where m_{ACG} and m_c are the average mass of neat ACG and the composite, respectively. The standard deviation of the three measurements is reported as the error for each formulation.

2.6. Humidity-Controlled Dynamic Mechanical Analysis (DMA-RH). Rectangular film sections 6.4 mm wide \times 20 mm long were tested in thin film tension mode on a TA Instruments (New Castle, DE) Q800 DMA-RH with humidity controlled chamber. Dry samples were clamped in the grips with 5 in. lb torque and subjected to a series of humidity sweeps at 25 °C while an oscillatory strain of 0.2% was applied at 1 Hz with minimum force set to 0.013 N. Each sample

was ramped from 5% to 95% relative humidity (RH), then back down to 5% RH, and then back up to 95% RH, with a soak time between 1 and 20 min per each 1% RH increment in the final two ramps. The final ramp from 5% to 95% RH is reported. The final negative and positive RH sweeps at the same rate exhibited a similar position of the peak in $\tan \delta$, indicating the sweep rate is slow enough to reach the equilibrium RH at which PAA glass transition temperature T_g equals room temperature.

2.7. Aqueous Swelling. Sections of dried films were weighed and then immersed in excess DI water or 100 mM phosphate buffered saline (Sigma-Aldrich). At timed intervals they were removed, dried lightly on paper towels, weighed on a microbalance, and then reimmersed in liquid.

2.8. Tensile Testing. The gauge section of each ASTM D412 Type D specimen was wrapped in a DIW-soaked paper towel for 3–5 min, such that the gauge section swelled to equilibrium while the grip sections remained dry. The specimen was clamped into an Instron 1122 frame with a 5 lb load cell (Honeywell) and serrated grips. Swollen dimensions were measured, and the sample was enclosed by a 250 mm tall \times 127 mm diameter plastic tube covered with water-soaked paper towels. A constant displacement rate of 24 mm/min was applied. Stress is reported as measured load divided by initial swollen cross-sectional area, while strain is reported as measured grip displacement divided by initial swollen gauge length.

2.9. Small-Angle Neutron Scattering (SANS). SBS-g-AA films (both protonated and sodium form) were shaken in excess deuterium oxide (D₂O) and dried prior to analysis to exchange PAA acid protons with deuterium. SANS data were collected on the CG-2 General Purpose SANS line on the High Flux Isotope Reactor, Oak Ridge National Laboratory (ORNL), at camera lengths of 0.3, 2.0, and 18 m, with neutron wavelength $\lambda = 4.75\text{ \AA}$, yielding a q range of 0.0038–0.61 Å⁻¹, where q is the magnitude of the scattering vector. SANS data were collected first on dry films stacked between quartz windows in demountable copper cells sealed with rubber O-rings. Samples were then removed from the cells, swollen to equilibrium in excess D₂O, and then reinserted into the cells. The remaining volume in the cells was filled with D₂O. The cells were held at 22 °C during all SANS data collection. The raw SANS data were corrected for transmission, background noise, and detector dark noise, prior to scaling to absolute

intensity. Data reduction was performed using Wavemetrics Igor Pro software and packages developed at ORNL and the National Institute for Standards and Technology (NIST). Analysis was performed using software available from Argonne National Laboratory.²⁹

2.10. Transmission Electron Microscopy (TEM). Samples for TEM were prepared using a Leica EM UC7 ultramicrotome with a Leica EM FC7 cryostage using a Diatome 35° diamond knife. Sections were cut at $-160\text{ }^{\circ}\text{C}$ to a thickness of 50–70 nm and warmed to room temperature under nitrogen to prevent ice formation. The sections were transferred to a Gatan Model 626 single tilt liquid nitrogen cryo-transfer TEM holder under a dry and room temperature atmosphere. The samples were then cooled to $-160\text{ }^{\circ}\text{C}$ using liquid nitrogen for the subsequent microscopy experiments. A JEOL JEM-2100F TEM and a Gatan 806 high-angle annular dark field scanning TEM (HAADF STEM) detector were used to collect dark field data from each sample. The TEM was operated at 200 kV, with a $40\text{ }\mu\text{m}$ condenser aperture, a HAADF STEM collection angle of 48–168 mrad, and spot size of 0.2 nm. Gatan Digital Micrograph version 1.85.1535 was used to collect and analyze the data.

3. RESULTS AND DISCUSSION

3.1. Synthesis and Molecular Characterization. Styrenic triblock copolymers such as polystyrene–polybutadiene–polystyrene (SBS) are important commodity thermoplastic elastomers used in applications such as adhesives, asphalt modifiers, tissue simulants, and many others.^{30–32} SBS forms a thermoreversible nanophase-separated morphology combining the rigidity and strength of glassy polystyrene with the ductility of polybutadiene rubber. Mechanical properties can be tuned over a very broad range by incorporating a midblock-selective solvent such as mineral oil, forming a nonaqueous thermoplastic elastomer gel (TPEG) which maintains dimensional stability and toughness due to glassy PS domains acting as physical cross-links in a soft matrix.^{30,33} Although SBS does not swell in water, the polybutadiene midblock features regular double bounds that are readily grafted by radical attack,^{34,35} offering the possibility of grafting a hydrophilic polymer to form a thermoplastic elastomer hydrogel, which could be expected to have good swelling ability and toughness due to the well-defined nanophase structure.

In this work, SBS was grafted with poly(acrylic acid) (PAA) via free-radical polymerization in dilute tetrahydrofuran (THF) solution, as shown in Figure 1a. Acrylic acid was chosen due to its low cost and ability to rapidly absorb large amounts of water, especially in the sodium salt form as used in superabsorbent polymers.³⁶ Furthermore, both SBS and PAA are biocompatible.^{37–41} Table 1 shows three series of products (labeled using the convention “grams of acrylic acid”—“series number”—note all formulations use a basis of 6 g of SBS). The first series consists of varying both monomer (acrylic acid) and initiator (AIBN) concentration in order to produce a systematically increasing ratio $[\text{AA}]_0/[\text{AIBN}]_0^{0.5}$. This ratio is proportional to molecular weight in a typical free radical polymerization, neglecting chain transfer.⁴²

A second series similar to the first was made to test repeatability of the polymerizations, and a third series was made to test the effect of different commercial SBS backbones: Vector 8508A and Vector 6241A (Dexco Polymers) contain 29 and 43 wt % styrene, respectively, giving V6241A a greater modulus and lower ductility than V8508A, while V8508A (68.4 kDa) has a 20% higher molecular weight than V6241A (56.8 kDa) and a 50% larger butadiene midblock, allowing it to incorporate a greater fraction of grafted PAA. Figure 1b plots the number-average molecular weight M_n of V8508A and the series 1 graft copolymers determined by size exclusion

chromatography (SEC) with differential refractometer and multiangle light scattering detectors, referred to here as multidetector SEC or MD-SEC. Also shown are MD-SEC results for a series of PAA homopolymers synthesized using the same formulations as series 1, but without SBS present. M_n of both the graft polymers and PAA homopolymers increase systematically with $[\text{AA}]_0/[\text{AIBN}]_0^{0.5}$, as predicted. These results are interpreted into a sketch of the graft copolymer topology in Figure 1c. As discussed in Supporting Information section S1, we estimate from MD-SEC measurements an approximate graft density of 28 ± 6 PAA grafts per SBS backbone, which does not appear to vary systematically with formulation in series 1. Based on this estimate, approximate volume fractions of each component are plotted in Figure 1d as a function of PAA M_n .

The graft copolymerization results in a large amount of ungrafted PAA, which was separated from the SBS-g-AA product. Ungrafted PAA is assumed equal in molecular weight to grafted PAA, since the polymerization is homogeneous when well-stirred and graft density is not sufficiently high to expect confinement effects.^{35,43} PAA is not commonly analyzed in THF,^{44,45} and MD-SEC measurements in THF gave erratic values for PAA formed in the presence of SBS, likely due to interactions with impurities such as talc added to SBS for processing (see details in Supporting Information section S1). On the other hand, relative molecular weight averages estimated using conventional calibration relative to polystyrene standards (referred to here as SEC-CC) followed the expected trends with respect to composition, swelling, and mechanical properties, but their values are not absolute. Since reliable data from both MD-SEC and SEC-CC were obtained for the pure PAA homopolymers produced in the absence of SBS (Figure 1b), a simple calibration curve was constructed to estimate quantitative molecular weight averages from SEC-CC results for other reactions. PAA molecular weight averages (number-average, M_n , and weight-average, M_w) estimated by this method are reported in Table 1 and elsewhere in the paper. Details of the correlation between MD-SEC and SEC-CC can be found in Supporting Information section S1.

Following extraction of ungrafted PAA in methanol, SBS-g-AA graft copolymers were dissolved in THF and cast into films. Selected films were converted to the sodium salt form of PAA by immersion in saturated sodium bicarbonate followed by thorough washing in DI water and drying. Films treated with divalent salts including Ca^{2+} and Zn^{2+} were formed by a similar method and will be discussed in section 3.5.

3.2. Humidity-Controlled Dynamic Mechanical Analysis. The softening of protonated (SBS-g-AA-H) and sodium form (SBS-g-AA- Na^+) graft copolymer films due to water uptake was studied using slow relative humidity (RH) sweeps in RH-controlled dynamic mechanical analysis (DMA-RH). Figures 2a and 2b show storage modulus E' and loss tangent $\tan \delta$, respectively, for series 1 films as a function of RH. With increasing RH there is a drop in E' of approximately 3 orders of magnitude, covering a similar range for all films including both H and Na^+ forms, excepting 10-1. $\tan \delta$ curves feature a prominent peak coinciding with this drop, suggesting the glass transition temperature T_g of the PAA phase decreases due to water absorption until it reaches room temperature at a characteristic value of RH, termed RH_g . This characteristic RH_g is similar for all films of a given form (H or Na^+), again excepting 10-1, but is about 15% lower for Na^+ films than H films, suggesting a portion of the water in Na^+ films has reduced

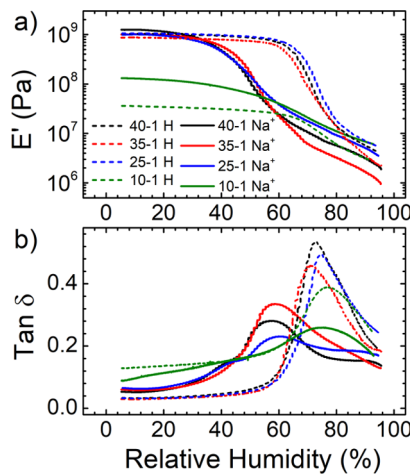


Figure 2. (a) Storage modulus and (b) loss tangent for series 1 SBS-g-AA films (H and Na⁺ forms) on final relative humidity (RH) sweep from 5% to 95% RH in humidity-controlled dynamic mechanical analysis (DMA-RH).

activity due to interactions with deprotonated acid groups. The unique behavior of 10-1 films in both forms, which exhibit lower dry modulus and higher RH_g than other compositions, is likely due to a lack of connectivity of microphase separated PAA domains, as will be shown in section 3.6.

As discussed in the **Introduction**, a critical requirement for a prehospital hemostatic dressing is sufficient flexibility to conform to a variety of wound geometries, first during application when the material must be flexible enough to be

inserted into wound cavities of varying size and second during compression inside the wound, where the material should maintain close contact with the contours of the damaged tissue in order to physically impede blood flow. To a first approximation, the maximum modulus allowable for a gel to conform to a given geometry can be estimated from simple contact mechanics. Inside the wound, we assume the relevant feature size is the blood vessels themselves, especially the arteries which have thick walls and are less collapsible than veins.⁴⁶ If we approximate the end of a torn artery as a hemisphere of radius R , we can estimate the depth δ of its penetration into the gel from

$$F = \frac{4}{3} E^* R^{1/2} \delta^{3/2} \quad (1)$$

where F is the applied force, such as that due to a person manually compressing the dressing into a wound. Here we have treated the artery and the gel as simple elastic solids and have neglected surface and adhesive forces because F is large. The reduced modulus E^* is defined by

$$\frac{1}{E^*} = \frac{1 - \nu_1^2}{E_1} + \frac{1 - \nu_2^2}{E_2} \quad (2)$$

where ν is Poisson's ratio, E is elastic modulus, and the subscripts 1 and 2 refer to the hydrogel and blood vessel, respectively. For the so-called elastic arteries, the largest and stiffest in the human body, E_2 is typically 1–2 MPa.⁴⁷ If we set $\delta = R$ (that is, the end of the artery completely penetrates the gel), under a load $F = 100$ N (a typical force exerted by a soldier's arm) and assume both gel and tissue are

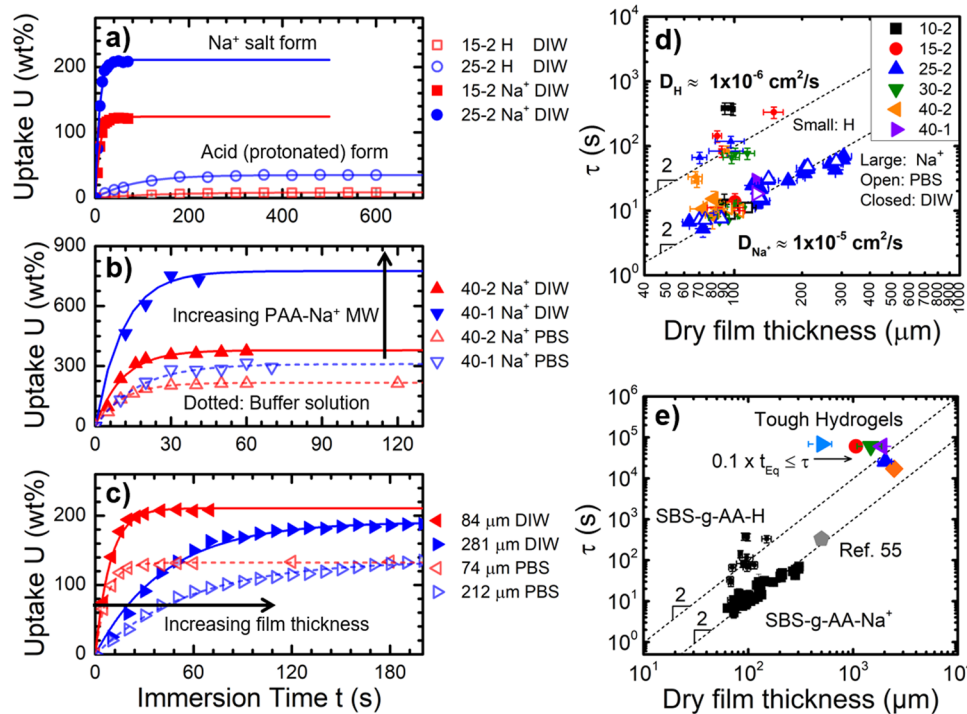


Figure 3. Mass uptake U as a function of immersion time t for (a) protonated (acid form) SBS-g-AA-H films and sodium salt SBS-g-AA-Na⁺ films of two different graft molecular weights in deionized water (DIW), (b) sodium salt SBS-g-AA-Na⁺ films of two different molecular weights in phosphate buffered saline (PBS, open symbols) and DIW (filled symbols), and (c) 25-2 Na⁺ films of different dry thicknesses in DIW (filled) and PBS (open). All curves in (a–c) are fits to eq 5. (d) Swelling time constant τ plotted as a function of dry film thickness a_d for various SBS-g-AA films in both DIW and PBS. Dotted lines are fits to eq 6 with diffusion coefficients D as indicated. (e) Comparison of the swelling kinetics of SBS-g-PAA films with tough hydrogels reported in the literature: ●,²⁸ ▲,⁵² ▼,²² ♦,¹⁹ ◀,⁵³ ▶,⁵⁴ gray ♪,⁵⁵

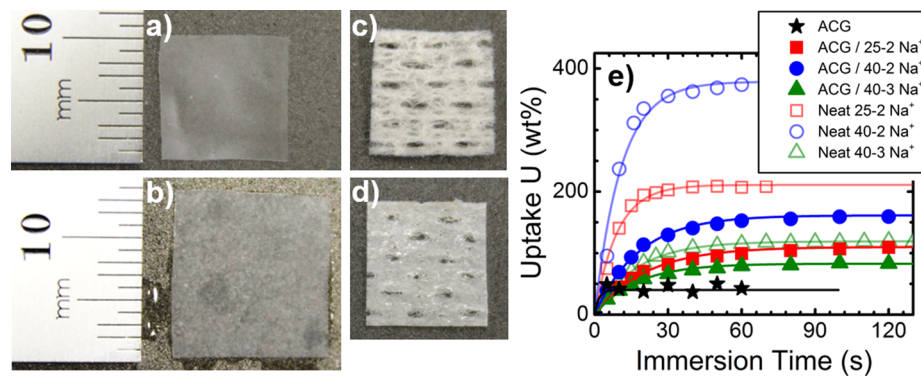


Figure 4. (a) Dry 25-2 Na⁺ film, (b) same film after immersion in DI water for 60 s, (c) dry Quikclot Advanced Clotting Gauze (ACG), (d) dry ACG/25-2 Na⁺ composite (c and d are same magnification as a and b), and (e) DI water uptake of ACG/SBS-g-AA Na⁺ composites compared to as-received ACG and neat polymer films. Lines are fits to eq 5.

incompressible ($\nu_1 = \nu_2 = 0.5$), we find that SBS-g-AA films in their hydrated state ($E_1 < 5 \times 10^6$ Pa) can fully conform around an artery with a maximum radius $R \approx 6.3$ mm. This is slightly smaller than the aorta ($R = 7\text{--}17$ mm)^{48,49} but greater than or equal to all other arteries, including the iliac arteries ($R = 4.5\text{--}6$ mm) and subclavian arteries ($R = 4\text{--}5$ mm),⁴⁹ both of which cross junctional regions where a substantial portion of lethaliities from hemorrhage occur on the battlefield.¹ Therefore, Figure 2 suggests the gels are sufficiently flexible in their hydrated state to conform to the vast majority of feature sizes likely to be critical for hemorrhage control. In the next section we will show that this hydration occurs very rapidly following immersion of the films into blood-like media.

3.3. Swelling of SBS-g-AA Films in Water and Saline.

The water uptake U , defined as

$$U = \frac{m_s - m_d}{m_d} \quad (3)$$

where subscripts s and d refer to swollen and dry mass m , respectively, was measured by immersing dry films of SBS-g-AA-H and SBS-g-AA-Na⁺ in excess deionized water (DIW) or phosphate buffered saline (PBS) in which the total ionic strength was about 0.1 M. U is plotted in Figure 3a–c for various films as a function of immersion time. Curves in Figure 3a–c are fits to a first-order kinetic model:^{50,51}

$$\frac{dU}{dt} = \frac{1}{\tau}(U_{Eq} - U) \quad (4)$$

With the solution

$$U(t) = U_{Eq}(1 - e^{-t/\tau}) \quad (5)$$

This model allows estimation of equilibrium uptake U_{Eq} for each sample. The swelling time constant τ is approximately 15% of t_{Eq} , the time to reach $U = U_{Eq}$, as illustrated in Figure S3a of the Supporting Information.

From Figure 3a,b it can be seen that U_{Eq} increases with graft molecular weight, and SBS-g-AA-Na⁺ films swell much faster and uptake much more water than SBS-g-AA-H films. Films immersed in PBS, which mimics the salinity of blood, swelled less than in DIW, consistent with a reduced osmotic pressure gradient. Nevertheless most Na⁺ formulations still swelled in excess of 100 wt % in PBS. Figure 3c shows that swelling time increased with film thickness in both DIW and PBS. Figure S3 shows swelling curves for additional samples, which follow the same trends as those in Figure 3a–c.

The well-known model of Tanaka and Fillmore⁵⁶ relates kinetics of gel swelling to the diffusion coefficient D of the polymer in the fluid:

$$\tau = \frac{a^2}{D} \quad (6)$$

where a is a linear dimension of the sample. Equation 6 is a useful approximation⁵⁷ for comparing trends among similar materials; however, diffusion coefficients reported here should only be taken as order of magnitude estimates. As illustrated in Figure 3d, using values of τ obtained from eq 5 and dry film thickness for a , our data agree well with the a^2 scaling predicted by eq 6, yielding diffusion coefficients of approximately 1×10^{-6} cm²/s for SBS-g-AA-H in DIW and approximately 1×10^{-5} cm²/s for SBS-g-AA-Na⁺ in both DI water and PBS. In other words, SBS-g-AA-Na⁺ swells about an order of magnitude faster than SBS-g-AA-H. This may be due to the greater osmotic pressure gradient for the polyelectrolyte SBS-g-AA-Na⁺ as well as the significant mobility of the PAA chains which are held in place only by their grafting site to the butadiene midblock, itself a rubbery link between glassy PS physical cross-links. Swelling of SBS-g-AA-Na⁺ is similarly rapid in both DIW and PBS, indicating that although equilibrium uptake is reduced due to the osmotic environment of PBS, swelling rate is not affected.

Many tough hydrogels reported in the literature are routinely incubated in swelling media (usually DIW) for several days to reach equilibrium. These samples are typically on the order of millimeters thick in the swollen state. Using the relationship

$$a_d = a_s \phi_p^{1/3} \quad (7)$$

we can estimate the dry thickness a_d of these materials from the swollen thickness a_s and polymer volume fraction ϕ_p :

$$\phi_p = \frac{1}{1 + U_{Eq}} \quad (8)$$

Assuming τ is approximately 10% of the time needed to reach swelling equilibrium (a conservative estimate according to eq 4), several tough hydrogels reported in the literature fall along the fit to eq 6 for SBS-g-AA-H, with an apparent diffusion coefficient $D \approx 1 \times 10^{-6}$ cm²/s, as shown in Figure 3e. From this analysis, typical tough hydrogels appear to swell about an order of magnitude slower than SBS-g-AA-Na⁺ studied here. However, it should be noted that detailed swelling kinetics are not reported for most tough hydrogels, likely because swelling

is undesirable in many hydrogel applications.⁵⁸ Interestingly, Sijbesma's group did recently report swelling kinetics from the dry state for a novel tough hydrogel.⁵⁵ Based on a fit to eq 5, τ for their material falls near the SBS-g-AA-Na⁺ data with $D \approx 1 \times 10^{-5} \text{ cm}^2/\text{s}$, plotted as the gray pentagon in Figure 3e. Their system bears further similarity to ours in that it is based on block copolymers held together by hydrophobic physical cross-links, and their mechanical properties as a function of ϕ_p are also comparable to ours, as reported below. On the other hand, Tanaka and Fillmore found $D \approx 3 \times 10^{-7} \text{ cm}^2/\text{s}$ for a common polyacrylamide gel.⁵⁶ Therefore, from the current literature, it is unclear to what extent swelling kinetics vary among different kinds of tough hydrogels, since such data are rarely reported. Given the value of rapid swelling for applications such as hemorrhage control, further research on this topic would be useful.

3.4. SBS-g-AA Composites Reinforced with Advanced Clotting Gauze (ACG). Fiber-reinforced hydrogel composites were formed by casting SBS-g-AA from THF onto QuikClot Advanced Clotting Gauze (ACG), a dry, kaolin-impregnated fabric sold commercially as a civilian equivalent to Combat Gauze. Figure 4a–d shows photographs of neat SBS-g-AA film in the dry and swollen states, as-received ACG, and an ACG/SBS-g-AA composite, respectively (the polymer in all cases is 25-2 Na⁺). Swelling was tested in DIW as above for Na⁺ form composites of 25-2, 40-2, and 40-3 containing approximately 1/3 ACG content by mass (Table 2). As shown in Figure 4e,

Table 2. ACG/SBS-g-AA Composite Weight Fractions and Swelling Parameters from Eq 5 Compared to Neat Films and As-Received ACG

sample	fiber content (wt %)	dry film thickness (μm)	U_E (wt %)	τ (s)
ACG	100	126 \pm 12	36 \pm 4	1.4 \pm 0.3
ACG/25-2 Na ⁺	36 \pm 3	310 \pm 10	112 \pm 6	20 \pm 2
ACG/40-2 Na ⁺	30 \pm 3	296 \pm 10	163 \pm 3	16 \pm 2
ACG/40-3 Na ⁺	31 \pm 2	316 \pm 17	82 \pm 1	17 \pm 1
neat 25-2 Na ⁺	0	73 \pm 10	210 \pm 7	7.3 \pm 2
neat 40-2 Na ⁺	0	80 \pm 6	492 \pm 121	11 \pm 3
neat 40-3 Na ⁺	0	142 \pm 6	123 \pm 5	18 \pm 2

water uptake of the composites was greater than that of as-received ACG but less than a neat film of the corresponding polymer. Interestingly, swelling time constants are only slightly larger than the neat polymers, despite the fact that composites are 2–4 times as thick as the neat films, as shown in Table 2. This is likely due to the porosity of the composites, shown in Figure 4d. Thus, the composites are able to swell to equilibrium within 1 min, suitable for the target application, and absorb 2–4 times as much water as the state of the art hemostatic dressing ACG.

3.5. Mechanical Properties. An effective hemostatic dressing must have sufficient cohesive energy (toughness) in the swollen state to be easily removed from a wound without breaking or leaving debris following treatment. While fracture energy (G or Γ) is an excellent quantitative measure of gel toughness,⁵⁹ the work of extension W , defined as the integral of the stress-strain curve from a uniaxial tensile test, has been found to scale similarly to G in many studies^{21,22,52} and is a good qualitative indicator of toughness for the purposes of this study.

Tensile measurements of swollen films were performed by soaking the gauge section of ASTM D412 type D dog bone film specimens with a DIW-saturated paper towel for 3–5 min to reach equilibrium. Grip sections of the specimens were kept dry to avoid breaking in the clamps. As shown in Figure 5a, the specimen was surrounded by DIW-saturated paper towels to provide a humidified environment and minimize evaporation during testing. DMA data in Figure S4 illustrate the effect of evaporation: at ambient conditions the modulus of Na⁺ form films began to increase after about 4–6 min due to drying, whereas the modulus of acid (H) form films increased after only 1 min, likely due to the greater water activity in H films as discussed in section 3.2. For tensile tests reported here we assume the humidified environment shown in Figure 5a suppresses evaporation for the duration of each test, the longest of which lasted 10–12 min.

Tensile properties of materials in this study, including Young's modulus E , ultimate tensile stress σ_{Ult} , and ultimate strain ε_{Ult} , are listed in Table 3. Comparing the two grades of as-received SBS, V6241A is roughly an order of magnitude stiffer and slightly less ductile than V8508A, as seen in Table 3 and Figure 5b. These properties, likely due to the greater styrene content of V6241A, are reflected in the series 3 graft polymers based on V6241A, which have much higher Young's modulus than the corresponding series 1 and 2 polymers based on V8508A (Table 3).

Figure 5c compares tensile curves of DIW-swollen SBS-g-AA-H and SBS-g-AA-Na⁺ films against Advanced Clotting Gauze, ACG. While ACG has a higher modulus than most of the swollen SBS-g-AA films, it is significantly less ductile. For the SBS-g-AA films, a systematic decrease of all tensile properties is generally observed with decreasing ϕ_p (increasing U_{Eq} , eq 8), as shown in Table 3. This trend of decreasing E , σ_{Ult} , and ε_{Ult} with decreasing ϕ_p is plotted in Figure S5 and compared to many hydrogels from the literature. Interestingly, Figure S5a shows that Young's modulus of SBS-g-AA films are among the highest reported for gels as a function of ϕ_p , which may be an effect of high functionality PS physical cross-links, as discussed in section 3.6.

Figure 6 compares W (toughness) of materials from this work against values reported for various hydrogels and nonaqueous gels in the literature as a function of ϕ_p . For papers that did not report a full stress–strain curve, we use the approximation $W \approx 1/2\sigma_{\text{Ult}}\varepsilon_{\text{Ult}}$ since the stress–strain curve of many gels approximates a right triangle.⁷⁰ Materials can be classified into “brittle” gels such as soft contact lenses,^{65,66} “tough” gels including state of the art amphiphilic hydrogels with reversible damage mechanisms,^{21,22} and “super-tough” gels, which includes a handful of outstanding performers such as double network hydrogels.²⁸ The swollen SBS-g-AA films generally fell into the “tough” category, with samples 25-2 Na⁺ and 40-3 Na⁺ approaching the “super-tough” regime. These two samples were 2.9 and 4.2 times as tough, respectively, as the state of the art hemostatic substrate ACG, even while absorbing 5.7 and 3.4 times as much water as ACG, respectively. In light of their rapid swelling in both water and PBS as discussed above, these formulations are intriguing candidates to augment the performance of gauze as a substrate for hemostatic agents such as kaolin and chitosan.

To that end, stress–strain curves of ACG/SBS-g-AA-Na⁺ composites are shown in Figure 5d. Young's moduli of the composites were much greater than the corresponding neat hydrogels, and in some cases even greater than as-received

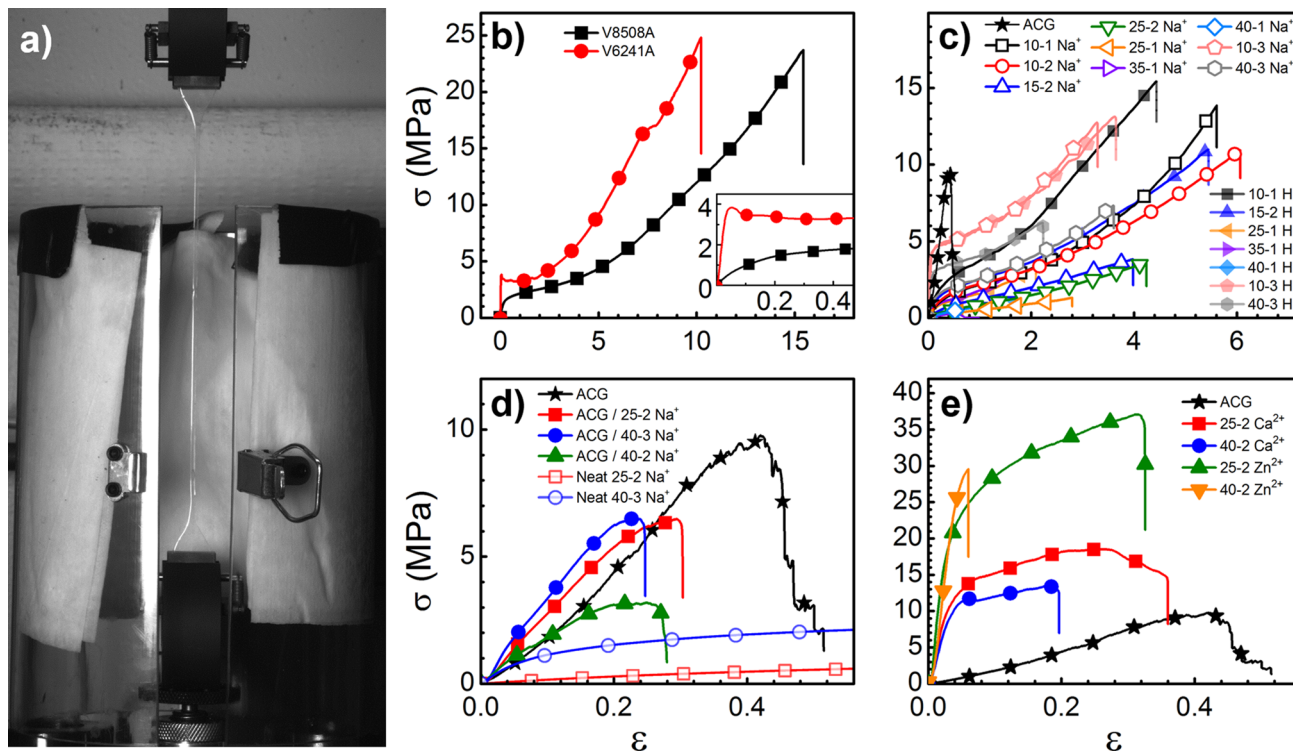


Figure 5. (a) Humidified tensile apparatus used to test swollen SBS-g-AA film specimens. Representative tensile stress-strain curves of (b) ungrafted SBS films cast from THF (inset shows small strain region), (c) wet SBS-g-AA films (H and Na⁺ form) and Advanced Clotting Gauze (ACG) swollen to equilibrium in DI water, (d) ACG/SBS-g-AA Na⁺ composites swollen to equilibrium in DI water, and (e) divalent salt cross-linked SBS-g-AA films (Ca²⁺ and Zn²⁺ form) after soaking in DI water.

Table 3. Mechanical Properties of SBS, SBS-g-AA, and ACG Composite Film Samples

sample	RH-DMA			tensile (swollen in DI water)					
	E' at 5% RH (MPa)	E' at 95% RH (MPa)	RH _g (%)	U _E (%)	φ _P (%)	E (MPa)	σ _{Ult} (MPa)	ε _{Ult} (mm/mm)	W (MJ/m ³)
ACG				37 ± 6	73 ± 3	27 ± 6	10 ± 2	0.40 ± 0.05	2.6 ± 0.6
V8508A	13	14		0	100	12.5 ± 1	23 ± 3.4	14.8 ± 0.7	138 ± 20
V6241A				0	100	140 ± 17	25 ± 2	10.5 ± 0.8	118 ± 16
10-1 H	36	3	78 ± 1	35 ± 3	74 ± 2	19.5 ± 5	14.7 ± 2	4.5 ± 0.6	33 ± 7.0
25-1 H	1050	5	71 ± 5	54 ± 2	65 ± 1	9.9 ± 6	5.7 ± 2	3.1 ± 0.8	9.1 ± 4.5
35-1 H	870	3	71 ± 1	109 ± 3	48 ± 1	7.9 ± 1.4	3.4 ± 1.3	2.0 ± 0.6	3.8 ± 2.2
15-2 H	234	9	81 ± 1	8.5 ± 1	92 ± 1	13 ± 1.4	10 ± 1.3	5 ± 0.5	25 ± 4.5
10-3 H				0.2 ± 0.1	100 ± 1	113 ± 12	12 ± 3	3.3 ± 0.8	25 ± 9.8
40-3 H	672	73	70 ± 2	18 ± 1	85 ± 1	84 ± 29	6.5 ± 2	2.4 ± 0.2	11 ± 3.9
10-1 Na ⁺	130	5	72 ± 1	25 ± 1	80 ± 1	5.7 ± 0.5	12.6 ± 2	5.6 ± 1.0	29 ± 8
25-1 Na ⁺	1170	2	60 ± 1	340 ± 6	23 ± 1	0.81 ± 0.06	0.97 ± 0.3	2.0 ± 0.6	1.1 ± 0.6
35-1 Na ⁺	980	1	58 ± 1	650 ± 44	13 ± 1	0.81 ± 0.04	0.35 ± 0.08	0.6 ± 0.2	0.12 ± 0.06
40-1 Na ⁺	1010	1	58 ± 1	742 ± 11	12 ± 1	0.96 ± 0.4	0.39 ± 0.15	0.5 ± 0.02	0.11 ± 0.05
10-2 Na ⁺	168	7	79 ± 1	26 ± 3	79 ± 2	7.5 ± 0.5	11 ± 3.8	6.1 ± 1.5	34 ± 16
15-2 Na ⁺	446	4	65 ± 1	89 ± 3	53 ± 1	2.6 ± 0.5	3.2 ± 0.9	3.3 ± 1	6.1 ± 2.6
25-2 Na ⁺	694	5	53 ± 1	210 ± 7	32 ± 1	1.6 ± 0.1	3.7 ± 0.9	4.3 ± 0.8	7.7 ± 2.9
10-3 Na ⁺	254	142	82 ± 1	3 ± 1	97 ± 1	140 ± 26	12 ± 2.7	3.3 ± 0.7	25 ± 8.3
40-3 Na ⁺	832	34	51 ± 2	123 ± 5	45 ± 1	15 ± 5	6.3 ± 1.3	3.1 ± 0.6	11 ± 3.5
ACG/25-2 Na ⁺				112 ± 6	47 ± 1	32 ± 4	3.1 ± 0.7	0.27 ± 0.04	1.0 ± 0.3
ACG/40-2 Na ⁺				163 ± 3	38 ± 1	22 ± 4	1.0 ± 0.3	0.27 ± 0.02	0.58 ± 0.2
ACG/40-3 Na ⁺				82 ± 1	55 ± 1	54 ± 8	3.1 ± 0.7	0.23 ± 0.03	0.89 ± 0.2
25-2 Ca ²⁺				8 ± 1	93 ± 1	617 ± 478	21 ± 13	0.26 ± 0.13	4.2 ± 1
40-2 Ca ²⁺				3 ± 0.5	97 ± 1	526 ± 189	18 ± 10	0.15 ± 0.07	2.5 ± 2
25-2 Zn ²⁺				0.5 ± 0.1	100 ± 1	958 ± 100	35 ± 5	0.33 ± 0.12	10 ± 5
40-2 Zn ²⁺				0.3 ± 0.1	100 ± 1	823 ± 79	29 ± 4.2	0.07 ± 0.01	0.93 ± 0.1

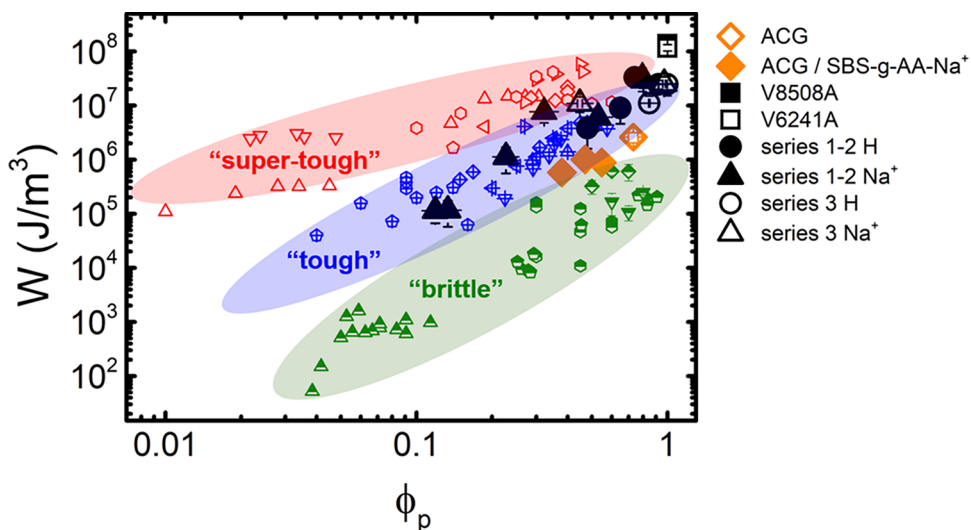


Figure 6. Work of extension W (toughness) for various gels plotted as a function of polymer volume fraction ϕ_p in gel. Legend indicates values from this work. Literature values include hydrogels: \square^{28} , \square^{21} , \triangle^{54} , \diamond^{60} , ∇^{53} , \triangleleft^{61} , \triangleright^{62} , crossed \square^{19} , crossed \square^{63} , crossed \triangle^{64} , crossed \diamond^{22} , crossed ∇^{52} , crossed \triangleright^{55} , half-filled \square^{65} , half-filled \triangle^{66} , half-filled \diamond^{67} and nonaqueous gels: crossed \triangleleft^{30} , half-filled \diamond^{68} , half-filled ∇^{69} .

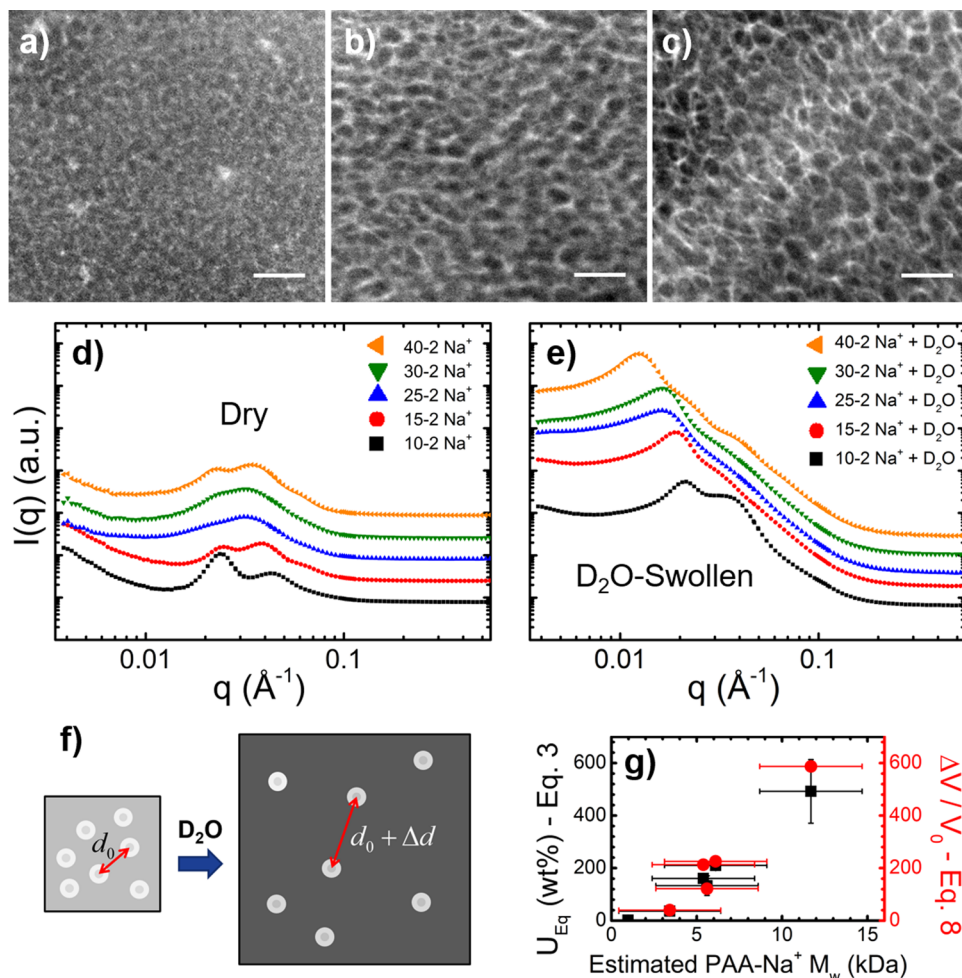


Figure 7. HAADF STEM images of unstained, microtomed sections from dry SBS-g-AA-Na⁺ films: (a) 10-1 Na⁺, (b) 25-2 Na⁺, (c) 40-1 Na⁺. Scale bars are 50 nm. (d) Small-angle neutron scattering (SANS) of series 2 Na⁺ films dry and (e) swollen in D_2O (shifted vertically for clarity in both graphs). (f) Schematic of morphology model used to derive eq 10. The matrix color change is intended to illustrate increased scattering contrast due to D_2O uptake. (g) Equilibrium DI water uptake U_{Eq} (black squares) of series 2 Na⁺ films as a function of estimated weight-average PAA molecular weight compared with volumetric swelling estimated from peak shift in SANS data according to eq 10 (red circles).

ACG (Table 3), despite containing more water (lower ϕ_p) than as-received ACG. However, their toughness W was less than that of ACG, decreasing systematically with water content following a similar scaling as the neat gels, as shown by the orange diamonds in Figure 6. While a few studies have recently reported fiber-reinforced hydrogel composites exhibiting “synergistic” toughness, that is, exceeding the toughness of either component alone,^{25,26} in this study that is not the case. One possible explanation is that the considerable swelling of the hydrogel (Figure 4) weakens fiber–matrix adhesion, reducing stress transfer at the interface and allowing fibers to pull out and fracture with reduced resistance or energy dissipation by the matrix. To date the greatest synergistic toughening effects have been observed in systems where the hydrogel matrix deswells,^{25,27} “squeezing” the fibers and increasing the friction of fiber pullout as well as transferring stress to the energy dissipative matrix in a large process zone around a crack tip. In the case of ACG/SBS-g-AA composites, ultimate elongation is reduced relative to the unmodified ACG fabric, whereas the stress is slightly greater at a given value of strain below ε_{Ult} . As shown in Figure S6, the absolute load supported by the composites is 4–5 times greater than ACG, on account of the greater thickness of the composites, implying stress transfer to the matrix is at least adequate at low strains. Therefore, we hypothesize that the fiber–matrix interface, already partially weakened due to swelling, debonds at a critical stress of 3–6 MPa, thus transferring load to the fibers that greatly exceeds their ultimate strength. This hypothesis explains the sharp, catastrophic failure observed for composites in Figure 5d, whereas unmodified ACG exhibits a more jagged failure curve characteristic of gradual breakage of fibers as they reach the threshold of their strength. Therefore, optimization of rapidly swelling, fiber-reinforced hydrogels for toughness may require novel designs, such as coiled or stretchable fibers that expand as the matrix swells to maintain strong adhesion.²⁶

It is interesting to explore the effect of other counterions besides sodium on the properties of SBS-g-AA polymers. Divalent salts have been shown to improve mechanical properties and modulate swellability of amphiphilic triblock copolymer hydrogels with poly(methacrylic acid) midblocks, by forming ionic cross-links between acid groups.⁶⁴ To determine the influence of added divalent salts on SBS-g-AA, films of 25-2-H and 40-2-H were treated with Ca^{2+} and Zn^{2+} , resulting in very stiff and strong films with a modulus 20–35 times greater than ACG (Figure 5e), albeit at a very low U_{Eq} (Table 3). In future work, a blend containing a small amount of divalent salt such as zinc with the sodium salt of SBS-g-AA may be a promising avenue of future research to moderately increase stiffness while maintaining high water contents. Alternatively, polycation additives may increase toughness by introducing a secondary network that distributes stress into a larger dissipation zone ahead of a crack tip, as was recently shown by Shull's group.⁷¹

3.6. SBS-g-AA Morphology. In order to better understand and improve upon the rapid swelling and good mechanical performance of SBS-g-AA Na^+ films, their nanoscale morphology was analyzed using high-angle annular dark field scanning transmission electron microscopy (HAADF STEM) and small-angle neutron scattering (SANS). Films for morphological analysis were cast in a saturated DIW and THF vapor environment, in an attempt to better resolve morphological features, whereas films for other tests were cast with no solvent annealing and faster evaporation. As shown in Figure S7, little

difference in tensile properties was found for films cast by the different methods, while subtle differences in the DMA-RH behavior were observed, suggesting films cast under saturated vapor feature a somewhat greater degree of phase separation.

Figure 7a–c shows HAADF STEM images of unstained sections from dry 10-1 Na^+ , 25-2 Na^+ , and 40-1 Na^+ , in which sodium-rich regions appear brighter than the surrounding dark organic phase(s) due to the presence of high-Z material (sodium). Although the starting SBS polymer was found to have a cylindrical morphology (as described in section S4 of the Supporting Information), no evidence of an ordered morphology was observed for SBS-g-AA materials via HAADF STEM. For 10-1 Na^+ , the bright sodium-rich regions do not appear fully connected nor well developed, consistent with the qualitative differences in DMA-RH behavior discussed in section 3.2, as well as the relatively slow and limited water uptake of this material. In contrast, 25-2 Na^+ and 40-1 Na^+ both appear to feature continuous networks of sodium-rich phase, suggesting the capability for very rapid water transport. This similar connectivity could explain why samples of sufficient PAA molecular weight all swell at approximately the same rate (Figure 3d).

Figure 7d compares SANS data from dry SBS-g-AA- Na^+ films to the same films swollen in deuterium oxide (D_2O , Figure 7e), revealing significant shifts of the primary peaks (q^*) to lower q upon D_2O uptake. The data in Figure 7e can be fit well using a core–shell sphere form factor combined with a Percus–Yevick type hard-sphere structure factor,^{72–74} (modeling data are given in section S4 of the Supporting Information). Therefore, the peak shifts can be interpreted using a simple model of spherical PS cores surrounded by PB shells in a matrix of PAA sodium salt, illustrated schematically in Figure 7f. In this picture the D_2O -swollen PAA matrix is shown as a darker shade of gray, illustrating that D_2O dominates the scattering contrast when present. Although not illustrated, PB tie chains between PS domains must also be present, given the mechanical toughness of the gels discussed above.

To a first approximation, the average spacing, d , between spherical domains can be estimated from the correlation length of the structure factor:

$$d = \frac{2\pi}{q^*} \quad (9)$$

In the initial, dry state, the PS domains are separated by an average distance d_0 . Uptake of D_2O then results in an increase in volume of the PAA- Na^+ phase, since PS and PB are assumed to be immiscible with D_2O , and therefore an increase in average spacing between hydrophobic domains to $d_0 + \Delta d$. Assuming isotropic swelling, the macroscopic volume change $\frac{\Delta V}{V_0}$ of the sample can then be calculated from

$$\frac{\Delta V}{V_0} = \left(1 + \frac{\Delta d}{d_0}\right)^3 - 1 \quad (10)$$

As shown in Figure 7g, $\frac{\Delta V}{V_0}$ estimated from the SANS data using eq 10 correlates very closely to mass uptake U_{Eq} in DIW, confirming both the validity of this simple model and the assumption that D_2O uptake is thermodynamically similar to that of H_2O . This model suggests that the relatively high toughness, stiffness, and strength of swollen SBS-g-AA films may be due in part to high functionality physical cross-links²³ in

the form of well-defined polystyrene domains chemically bonded via ductile polybutadiene linkages to a highly swollen, continuous PAA matrix.

3.7. Conclusions. Work over the past 15 years has demonstrated that a safe prehospital battlefield hemostatic dressing requires a cohesive substrate that is flexible when dry, rapidly absorbs a large amount of water, and remains tough while swollen for intact removal. With these conditions in mind, we have used simple free-radical graft polymerization of acrylic acid onto commercial thermoplastic elastomers to design a rubber capable of rapidly swelling into a tough hydrogel. These capabilities are due to a nanophase-separated structure featuring glassy physical cross-links and rubbery linkages supporting a continuous mobile ionic phase. The formulation can be tuned to balance high and fast swelling with good mechanical properties, exceeding both the water uptake and toughness of a state of the art hemostatic gauze dressing, while apparently swelling up to an order of magnitude faster than many tough hydrogels in the literature. Composites featuring the polymer reinforced with a commercial gauze dressing show improved swelling and Young's modulus, but the fiber–matrix interface may need further optimization to maximize toughness. These results illustrate the potential of this material platform to improve performance of advanced hemostatic dressings by increasing blood absorption to stabilize massively hemorrhaging wounds faster, while maintaining mechanical integrity for safe removal following treatment.

■ ASSOCIATED CONTENT

Supporting Information

The Supporting Information is available free of charge on the ACS Publications website at DOI: [10.1021/acs.macromol.8b00428](https://doi.org/10.1021/acs.macromol.8b00428).

Details of synthesis, molecular characterization, swelling, mechanical testing, and analysis of scattering data ([PDF](#))

■ AUTHOR INFORMATION

Corresponding Authors

*E-mail randy.a.mrozek.civ@mail.mil (R.A.M.).

*E-mail joseph.l.lenhart.civ@mail.mil (J.L.L.).

ORCID

Erich D. Bain: [0000-0002-2195-7798](https://orcid.org/0000-0002-2195-7798)

Frederick L. Beyer: [0000-0003-0253-2134](https://orcid.org/0000-0003-0253-2134)

Alice M. Savage: [0000-0003-0167-4966](https://orcid.org/0000-0003-0167-4966)

Mark D. Dadmun: [0000-0003-4304-6087](https://orcid.org/0000-0003-4304-6087)

Author Contributions

E.D.B. and T.R.L. contributed equally to this work.

Notes

The authors declare no competing financial interest.

■ ACKNOWLEDGMENTS

We acknowledge Dr. Lilin He for assistance with SANS measurements, Dr. Scott Walck for assistance with TEM, and Chris Gold, Brad Leighliter, and Dr. Sam Price for early contributions to this project. A.M.S. was supported in part by the Postgraduate Research Participation Program at the U.S. Army Research Laboratory, administered by the Oak Ridge Institute of Science and Education through an interagency agreement between the U.S. Department of Energy and Army Research Laboratory (Contract ORISE 1120-1120-99). M.D.D. and H.J.M. were supported by the Department of Energy, Basic

Energy Sciences, Materials Sciences and Engineering Division. A portion of this research used resources at the High Flux Isotope Reactor, a DOE Office of Science User Facility operated by the Oak Ridge National Laboratory.

■ REFERENCES

- (1) Eastridge, B. J.; Mabry, R. L.; Seguin, P.; Cantrell, J.; Tops, T.; Uribe, P.; Mallett, O.; Zubko, T.; Oetjen-Gerdes, L.; Rasmussen, T. E.; Butler, F. K.; Kotwal, R. S.; Holcomb, J. B.; Wade, C. E.; Champion, H.; Lawnick, M.; Moores, L.; Blackbourne, L. H. Death on the battlefield (2001–2011): Implications for the future of combat casualty care. *J. Trauma Acute Care Surg.* **2012**, *73* (6), S431–S437.
- (2) Eastridge, B. J.; Hardin, M.; Cantrell, J.; Oetjen-Gerdes, L.; Zubko, T.; Mallak, C.; Wade, C. E.; Simmons, J.; Mace, J.; Mabry, R.; Bolenbaucher, R.; Blackbourne, L. H. Died of Wounds on the Battlefield: Causation and Implications for Improving Combat Casualty Care. *J. Trauma* **2011**, *71* (1), S4–S8.
- (3) Granville-Chapman, J.; Jacobs, N.; Midwinter, M. J. Pre-hospital haemostatic dressings: a systematic review. *Injury* **2011**, *42* (5), 447–59.
- (4) Curry, N.; Hopewell, S.; Doree, C.; Hyde, C.; Brohi, K.; Stanworth, S. The acute management of trauma hemorrhage: a systematic review of randomized controlled trials. *Critical Care* **2011**, *15*, R92.
- (5) Alam, H. B.; Burris, D.; DaCorta, J. A.; Rhee, P. Hemorrhage control in the battlefield: role of new hemostatic agents. *Mil. Med.* **2005**, *170* (1), 63–69.
- (6) Pusateri, A. E.; Holcomb, J. B.; Kheirabadi, B. S.; Alam, H. B.; Wade, C. E.; Ryan, K. L. Making sense of the preclinical literature on advanced hemostatic products. *J. Trauma* **2006**, *60* (3), 674–82.
- (7) Littlejohn, L.; Bennett, B. L.; Drew, B. Application of current hemorrhage control techniques for backcountry care: part two, hemostatic dressings and other adjuncts. *Wilderness Environ. Med.* **2015**, *26* (2), 246–54.
- (8) Ellis-Behnke, R. G.; Liang, Y. X.; Tay, D. K.; Kau, P. W.; Schneider, G. E.; Zhang, S.; Wu, W.; So, K. F. Nano hemostat solution: immediate hemostasis at the nanoscale. *Nanomedicine* **2006**, *2* (4), 207–15.
- (9) Luo, Z.; Wang, S.; Zhang, S. Fabrication of self-assembling D-form peptide nanofiber scaffold d-EAK16 for rapid hemostasis. *Biomaterials* **2011**, *32* (8), 2013–20.
- (10) Chaturvedi, A.; Dowling, M. B.; Gustin, J. P.; Scalea, T. M.; Raghavan, S. R.; Pasley, J. D.; Narayan, M. Hydrophobically modified chitosan gauze: a novel topical hemostat. *J. Surg. Res.* **2017**, *207*, 45–52.
- (11) Dowling, M. B.; Kumar, R.; Keibler, M. A.; Hess, J. R.; Bochicchio, G. V.; Raghavan, S. R. A self-assembling hydrophobically modified chitosan capable of reversible hemostatic action. *Biomaterials* **2011**, *32* (13), 3351–7.
- (12) Hsu, B. B.; Hagerman, S. R.; Jamieson, K.; Castleberry, S. A.; Wang, W.; Holler, E.; Ljubimova, J. Y.; Hammond, P. T. Multifunctional Self-Assembled Films for Rapid Hemostat and Sustained Anti-infective Delivery. *ACS Biomater. Sci. Eng.* **2015**, *1* (3), 148–156.
- (13) Shukla, A.; Fang, J. C.; Puranam, S.; Jensen, F. R.; Hammond, P. T. Hemostatic multilayer coatings. *Adv. Mater.* **2012**, *24* (4), 492–6.
- (14) Chan, L. W.; Wang, X.; Wei, H.; Pozzo, L. D.; White, N. J.; Pun, S. H. A synthetic fibrin cross-linking polymer for modulating clot properties and inducing hemostasis.pdf>. *Sci. Transl. Med.* **2015**, *7* (277), 277ra29.
- (15) Landolina, J. A. In-situ cross-linkable polymeric compositions and methods thereof. US Patent WO2013071235, May 16, 2013.
- (16) Arnaud, F.; Teranishi, K.; Tomori, T.; Carr, W.; McCarron, R. Comparison of 10 hemostatic dressings in a groin puncture model in swine. *J. Vasc. Surg.* **2009**, *50* (3), 632–9 639 e1.
- (17) Kheirabadi, B. S.; Mace, J. E.; Terrazas, I. B.; Fedyk, C. G.; Estep, J. S.; Dubick, M. A.; Blackbourne, L. H. Safety evaluation of new hemostatic agents, smectite granules, and kaolin-coated gauze in a

- vascular injury wound model in swine. *J. Trauma* **2010**, *68* (2), 269–78.
- (18) Okumura, Y.; Ito, K. The polyrotaxane gel: a topological gel by figure-of-eight crosslinks. *Adv. Mater.* **2001**, *13* (7), 485–487.
- (19) Haraguchi, K.; Takehisa, T. Nanocomposite hydrogels: a unique organic-inorganic network structure with extraordinary mechanical, optical, and swelling-deswelling properties. *Adv. Mater.* **2002**, *14* (16), 1120–1124.
- (20) Gong, J. P.; Katsuyama, Y.; Kurokawa, T.; Osada, Y. Double network hydrogels with extremely high mechanical strength. *Adv. Mater.* **2003**, *15* (14), 1155–1158.
- (21) Sun, J. Y.; Zhao, X.; Illeperuma, W. R.; Chaudhuri, O.; Oh, K. H.; Mooney, D. J.; Vlassak, J. J.; Suo, Z. Highly stretchable and tough hydrogels. *Nature* **2012**, *489* (7414), 133–6.
- (22) Sun, L.; Kurokawa, T.; Kuroda, S.; Ihsan, A.; Akasaki, T.; Sato, K.; Haque, M.; Nakajima, T.; Gong, J. Physical hydrogels composed of polyampholytes demonstrate high toughness and viscoelasticity. *Nat. Mater.* **2013**, *12*, 932–937.
- (23) Zhao, X. Multi-scale multi-mechanism design of tough hydrogels: building dissipation into stretchy networks. *Soft Matter* **2014**, *10* (5), 672–87.
- (24) Illeperuma, W. R. K.; Sun, J. Y.; Suo, Z.; vlassak, J. J. Fiber-reinforced tough hydrogels. *Extreme Mechanics Letters* **2014**, *1*, 90–96.
- (25) Huang, Y.; King, D. R.; Sun, T. L.; Nonoyama, T.; Kurokawa, T.; Nakajima, T.; Gong, J. P. Energy-dissipative matrices enable synergistic toughening in fiber reinforced soft composites. *Adv. Funct. Mater.* **2017**, *27*, 1605350.
- (26) Lin, S.; Cao, C.; Wang, Q.; Gonzalez, M.; Dolbow, J. E.; Zhao, X. Design of stiff, tough and stretchy hydrogel composites via nanoscale hybrid crosslinking and macroscale fiber reinforcement. *Soft Matter* **2014**, *10* (38), 7519–27.
- (27) King, D. R.; Sun, T. L.; Huang, Y.; Kurokawa, T.; Nonoyama, T.; Crosby, A. J.; Gong, J. P. Extremely tough composites from fabric reinforced polyampholyte hydrogels. *Mater. Horiz.* **2015**, *2*, 584–591.
- (28) Itagaki, H.; Kurokawa, T.; Furukawa, H.; Nakajima, T.; Katsumoto, Y.; Gong, J. P. Water-Induced Brittle-Ductile Transition of Double Network Hydrogels. *Macromolecules* **2010**, *43* (22), 9495–9500.
- (29) Ilavsky, J.; Jemian, P. R. Irena: tool suite for modeling and analysis of small-angle scattering. *J. Appl. Crystallogr.* **2009**, *42* (2), 347–353.
- (30) Mrozek, R. A.; Leighliter, B.; Gold, C. S.; Beringer, I. R.; Yu, J. H.; VanLandingham, M. R.; Moy, P.; Foster, M. H.; Lenhart, J. L. The relationship between mechanical properties and ballistic penetration depth in a viscoelastic gel. *J. Mech Behav Biomed. Mater.* **2015**, *44*, 109–20.
- (31) Drobny, J. G. *Handbook of Thermoplastic Elastomers*; Elsevier: 2014.
- (32) Jasso, M.; Bakos, D.; MacLeod, D.; Zanzotto, L. Preparation and properties of conventional asphalt modified by physical mixtures of linear SBS and montmorillonite clay. *Construction and Building Materials* **2013**, *38*, 759–765.
- (33) Laurer, J. H.; Mulling, J. F.; Khan, S. A.; Spontak, R. J.; Bukovnik, R. Thermoplastic elastomer gels. I. effects of composition and processing on morphology and gel behavior. *J. Polym. Sci., Part B: Polym. Phys.* **1998**, *36*, 2379–2391.
- (34) Huang, N.-J.; Sundberg, D. C. Fundamental studies of grafting reactions in free radical copolymerization. I. A detailed kinetic model for solution polymerization. *J. Polym. Sci., Part A: Polym. Chem.* **1995**, *33*, 2533–2549.
- (35) Huang, N.-J.; Sundberg, D. C. Fundamental studies of grafting reactions in free radical copolymerization. II. Grafting of styrene, acrylate, and methacrylate monomers onto cis-polybutadiene using AIBN initiator in solution polymerization. *J. Polym. Sci., Part A: Polym. Chem.* **1995**, *33*, 2551–2570.
- (36) Buchholz, F. L. Superabsorbent polymers: an idea whose time has come. *J. Chem. Educ.* **1996**, *73* (6), 512–515.
- (37) Ranade, S. V.; Richard, R. E.; Helmus, M. N. Styrenic block copolymers for biomaterial and drug delivery applications. *Acta Biomater.* **2005**, *1* (1), 137–144.
- (38) Yang, J. M.; Tsai, S. C. Biocompatibility of epoxidized styrene–butadiene–styrene block copolymer membrane. *Mater. Sci. Eng., C* **2010**, *30* (8), 1151–1156.
- (39) Sato, H.; Nakajima, A.; Hayashi, T.; Chen, G. W.; Noishiki, Y. Microheterophase structure, permeability, and biocompatibility of A-B-A triblock copolymer membranes composed of poly(γ -ethyl L-glutamate) as the A component and polybutadiene as the B component. *J. Biomed. Mater. Res.* **1985**, *19* (9), 1135–1155.
- (40) De Giglio, E.; Cafagna, D.; Ricci, M.; Sabbatini, L.; Cometa, S.; Ferretti, C.; Mattioli-Belmonte, M. Biocompatibility of Poly(Acrylic Acid) Thin Coatings Electro-synthesized onto TiAlV-based Implants. *J. Bioact. Compat. Polym.* **2010**, *25*, 374–391.
- (41) Ahmed, A.-F.; Zakaria, K. M. Synthesis, characterization, and biocompatibility of poly (acrylic acid/methyl methacrylate)-grafted-poly (ethylene-co-tetrafluoroethylene) film for prosthetic cardiac valves. *Colloid Polym. Sci.* **2014**, *292* (12), 3301–3310.
- (42) Odian, G. *Principles of Polymerization*, 4th ed.; John Wiley & Sons: Hoboken, NJ, 2004.
- (43) Bain, E. D.; Dawes, K.; Ozcam, A. E.; Hu, X.; Gorman, C. B.; Srogl, J.; Genzer, J. Surface-initiated polymerization by means of novel, stable, non-ester based radical initiator. *Macromolecules* **2012**, *45*, 3802–3815.
- (44) Lacik, I.; Stach, M.; Kasák, P.; Semák, V.; Uhelská, L.; Chovancová, A.; Reinhold, G.; Kilz, P.; Delaittre, G.; Charleux, B.; Chaduc, I.; D'Agosto, F.; Lansalot, M.; Gaborieau, M.; Castignolles, P.; Gilbert, R. G.; Szablan, Z.; Barner-Kowollik, C.; Hesse, P.; Buback, M. SEC Analysis of Poly(Acrylic Acid) and Poly(Methacrylic Acid). *Macromol. Chem. Phys.* **2015**, *216* (1), 23–37.
- (45) Penzel, E.; Goetz, N. Solution properties of polyacrylic esters I. light scattering and viscosity measurements in tetrahydrofuran. *Angew. Makromol. Chem.* **1990**, *178*, 191–200.
- (46) Lee, D.-K.; Ahn, K.-S.; Kang, C. H.; Cho, S. B. Ultrasonography of the lower extremity veins: anatomy and basic approach. *Ultrasonography* **2017**, *36* (2), 120–130.
- (47) Lang, R. M.; Cholley, B. P.; Korcarz, C.; Marcus, R. H.; Shroff, S. G. Measurement of regional elastic properties of the human aorta. A new application of transesophageal echocardiography with automated border detection and calibrated subclavian pulse tracings. *Circulation* **1994**, *90* (4), 1875–1882.
- (48) Lickfett, L.; Dickfeld, T.; Kato, R.; Tandri, H.; Vasamreddy, C. R.; Berger, R.; Bluemke, D.; Luderitz, B.; Halperin, H.; Calkins, H. Changes of pulmonary vein orifice size and location throughout the cardiac cycle: dynamic analysis using magnetic resonance cine imaging. *J. Cardiovasc Electrophysiol* **2005**, *16* (6), 582–8.
- (49) Kahraman, H.; Ozaydin, M.; Varol, E.; Aslan, S. M.; Dogan, A.; Altinbas, A.; Demir, M.; Gedikli, O.; Acar, G.; Ergene, O. The Diameters of the Aorta and Its Major Branches in Patients with Isolated Coronary Artery Ectasia. *Texas Heart Inst. J.* **2006**, *33* (4), 463–468.
- (50) Schott, H. Kinetics of swelling of polymers and their gels. *J. Pharm. Sci.* **1992**, *81* (5), 467–470.
- (51) Andrews, D. H.; Johnston, J. The rate of absorption of water by rubber. *J. Am. Chem. Soc.* **1924**, *46*, 640–650.
- (52) Li, J.; Suo, Z.; Vlassak, J. J. Stiff, strong, and tough hydrogels with good chemical stability. *J. Mater. Chem. B* **2014**, *2* (39), 6708–6713.
- (53) Zhang, S.; Shi, Z.; Xu, H.; Ma, X.; Yin, J.; Tian, M. Revisiting the mechanism of redox-polymerization to build the hydrogel with excellent properties using a novel initiator. *Soft Matter* **2016**, *12* (9), 2575–82.
- (54) Song, G.; Zhang, L.; He, C.; Fang, D.-C.; Whitten, P. G.; Wang, H. Facile Fabrication of Tough Hydrogels Physically Cross-Linked by Strong Cooperative Hydrogen Bonding. *Macromolecules* **2013**, *46* (18), 7423–7435.
- (55) Mihajlovic, M.; Staropoli, M.; Appavou, M. S.; Wyss, H. M.; Pyckhout-Hintzen, W.; Sijbesma, R. P. Tough Supramolecular

- Hydrogel Based on Strong Hydrophobic Interactions in a Multiblock Segmented Copolymer. *Macromolecules* **2017**, *50* (8), 3333–3346.
- (56) Tanaka, T.; Fillmore, D. J. Kinetics of swelling of gels. *J. Chem. Phys.* **1979**, *70*, 1214–1218.
- (57) Keener, J. P.; Sircar, S.; Fogelson, A. L. Influence of the standard free energy on swelling kinetics of gels. *Phys. Rev. E Stat Nonlin Soft Matter Phys.* **2011**, *83* (4), 041802.
- (58) Kamata, H.; Kushiro, K.; Takai, M.; Chung, U.-i.; Sakai, T. Non-Osmotic Hydrogels: A Rational Strategy for Safely Degradable Hydrogels. *Angew. Chem., Int. Ed.* **2016**, *55* (32), 9282–9286.
- (59) Creton, C.; Ciccotti, M. Fracture and adhesion of soft materials: a review. *Rep. Prog. Phys.* **2016**, *79* (4), 046601.
- (60) Lin, P.; Ma, S.; Wang, X.; Zhou, F. Molecularly engineered dual-crosslinked hydrogel with ultrahigh mechanical strength, toughness, and good self-recovery. *Adv. Mater.* **2015**, *27* (12), 2054–9.
- (61) Su, Q.; Wang, Y.; Guan, S.; Zhang, H.; Gao, G. H.; Zhu, X. Rapid formation of highly stretchable and notch-insensitive hydrogels. *RSC Adv.* **2016**, *6* (36), 30570–30576.
- (62) Yang, N.; Yang, H.; Shao, Z.; Guo, M. Ultrastrong and Tough Supramolecular Hydrogels from Multiurea Linkage Segmented Copolymers with Tractable Processability and Recyclability. *Macromol. Rapid Commun.* **2017**, *38* (17), 1700275.
- (63) Sakai, T.; Matsunaga, T.; Yamamoto, Y.; Ito, C.; Yoshida, R.; Suzuki, S.; Sasaki, N.; Shibayama, M.; Chung, U. Design and fabrication of a high-strength hydrogel with ideally homogeneous network structure from tetrahedron-like macromonomers. *Macromolecules* **2008**, *41*, 5379–5384.
- (64) Henderson, K. J.; Zhou, T. C.; Otim, K. J.; Shull, K. R. Ionically Cross-Linked Triblock Copolymer Hydrogels with High Strength. *Macromolecules* **2010**, *43* (14), 6193–6201.
- (65) Tranoudis, I.; Efron, N. Tensile properties of soft contact lens materials. *Cont Lens Anterior Eye* **2004**, *27* (4), 177–91.
- (66) Johnson, B. D.; Beebe, D. J.; Crone, W. C. Effects of swelling on the mechanical properties of a pH-sensitive hydrogel for use in microfluidic devices. *Mater. Sci. Eng., C* **2004**, *24* (4), 575–581.
- (67) Djonagic, J.; Petrovi, Z. S. Semi-interpenetrating polymer networks composed of poly(N-isopropyl acrylamide) and polyacrylamide hydrogels. *J. Polym. Sci., Part B: Polym. Phys.* **2004**, *42* (21), 3987–3999.
- (68) Mrozek, R. A.; Cole, P. J.; Otim, K. J.; Shull, K. R.; Lenhart, J. L. Influence of solvent size on the mechanical properties and rheology of polydimethylsiloxane-based polymeric gels. *Polymer* **2011**, *52* (15), 3422–3430.
- (69) Mrozek, R. A.; Cole, P. J.; Cole, S. M.; Schroeder, J. L.; Schneider, D. A.; Hedden, R. C.; Lenhart, J. L. Design of nonaqueous polymer gels with broad temperature performance: Impact of solvent quality and processing conditions. *J. Mater. Res.* **2010**, *25* (06), 1105–1117.
- (70) Naficy, S.; Brown, H.; Razal, J.; Spinks, G.; Whitten, P. Progress Toward Robust Polymer Hydrogels. *Aust. J. Chem.* **2011**, *64*, 1007–1025.
- (71) Chen, Y.; Shull, K. R. High-Toughness Polycation Cross-Linked Triblock Copolymer Hydrogels. *Macromolecules* **2017**, *50* (9), 3637–3646.
- (72) Percus, J. K.; Yevick, G. J. Analysis of Classical Statistical Mechanics by Means of Collective Coordinates. *Phys. Rev.* **1958**, *110* (1), 1–13.
- (73) Kinning, D. J.; Thomas, E. L. Hard-sphere interactions between spherical domains in diblock copolymers. *Macromolecules* **1984**, *17* (9), 1712–1718.
- (74) Visser, S. A.; Cooper, S. L. Analysis of small-angle x-ray scattering data for model polyurethane ionomers: evaluation of hard-sphere models. *Macromolecules* **1991**, *24* (9), 2584–2593.